Brain Topogr
DOI 10.1007/s10548-017-0581-z

ORIGINAL PAPER

White Matter Connectivity Pattern Associate with Characteristics of Scalp EEG Signals

Jinnan Gong[1] · Cheng Luo[1] · Xuebin Chang[1] · Rui Zhang[1] · Benjamin Klugah-Brown[1] · Lanjin Guo[1] · Peng Xu[1] · Dezhong Yao[1]

Received: 7 September 2016 / Accepted: 27 July 2017

Abstract The rhythm of electroencephalogram (EEG) depends on the neuroanatomical-based parameters such as white matter (WM) connectivity. However, the impacts of these parameters on the specific characteristics of EEG have not been clearly understood. Previous studies demonstrated that, these parameters contribute the inter-subject differences of EEG during performance of specific task such as motor imagery (MI). Though researchers have worked on this phenomenon, the idea is yet to be understood in terms of the mechanism that underlies such differences. Here, to tackle this issue, we began our investigations by first examining the structural features related to scalp EEG characteristics, which are event-related desynchronizations (ERDs), during MI using diffusion MRI. Twenty-four right-handed subjects were recruited to accomplish MI tasks and MRI scans. Based on the high spatial resolution of the structural and diffusion images, the motor-related WM links, such as basal ganglia (BG)-primary somatosensory cortex (SM1) pathway and supplementary motor area (SMA)-SM1 connection, were reconstructed by using probabilistic white matter tractography. Subsequently, the relationships of WM characteristics with EEG signals were investigated. These analyses demonstrated that WM pathway characteristics, including the connectivity strength and the positional characteristics of WM connectivity on SM1 (defined by the gyrus-sulcus ratio of connectivity, GSR), have a significant impact on ERDs when doing MI. Interestingly, the high GSR of WM connections between SM1 and BG were linked to the better ERDs. These results therefore, indicated that the connectivity in the gyrus of SM1 interacted with MI network which played the critical role for the scalp EEG signal extraction of MI to a great extent. The study provided the coupling mechanism between structural and dynamic physiological features of human brain, which would also contribute to understanding individual differences of EEG in MI-brain computer interface.

Keywords Diffusion MRI · Eeg · White matter connectivity · Motor imagery · Brain-computer interface

Introduction

The rhythm of scalp electroencephalogram (EEG) depends on the neuroanatomical-based parameters. For example, Whitford et al. demonstrated that the EEG activity, especially in the slow-wave band, changes along with the alteration of gray matter volume from 10 to 30 years (Whitford et al. 2006). Pedro et al. found a relationship between fractional anisotropy and alpha peak, suggesting that the alpha frequency might be controlled by the period of cortico-thalamocortical loop (Valdés-Hernández et al. 2010). The above mentioned studies suggested that, the inter-subject differences of resting states EEG may associated with neuroanatomical characteristics. However, during performance

Electronic supplementary material The online version of this article (doi:10.1007/s10548-017-0581-z) contains supplementary material, which is available to authorized users.

✉ Cheng Luo
chengluo@uestc.edu.cn

✉ Dezhong Yao
dyao@uestc.edu.cn

[1] Key Laboratory for NeuroInformation of Ministry of Education, Center for Information in Medicine, High-Field Magnetic Resonance Brain Imaging Key Laboratory of Sichuan Province, School of Life Science and Technology, University of Electronic Science and Technology of China, Chengdu, China

Published online: 07 August 2017

of specific tasks, such as motor imagery (MI), may produce special EEG signals.

Brain-computer interfaces (BCI) is an implication of EEG signal extraction in clinical and engineering fields. BCI represent a technology that provides direct communication between the brain and the external world and have been used in an increasing number of domains, such as in rehabilitation and disability aids (Kubler et al. 2005; Daly and Wolpaw 2008; Galán et al. 2008; Müller-Putz et al. 2014), over the past decades. To achieve interaction with the peripheral equipment through BCI, the key techniques includes an extraction of neural activity signals and a selection of a proper model to classify the signals for the interaction with the computer (Ramoser et al. 2000). Usually, EEG, especially the motor imagery (MI) induced EEG, provides a non-invasive approach to detect the BCI features. The neurophysiological basis of MI is that the energy of the sensorimotor cortex in Mu and Beta rhythm will be reduced or elevated compared to spontaneous EEG, in performing MI. The changes of EEG energy can be measured by event-related desynchronization (ERD) and the event-related synchronization (ERS), respectively. In order to actualize the motor imagery based BCI (MI-BCI), the detection of frequency specific changes of the ongoing EEG activity, including ERD and ERS, are usually been involved. For example, the sensory motor rhythms (SMR) desynchronization in the 8–30 Hz frequency serves as the main classification feature in MI-BCI. Nevertheless, although the classifying mode in BCI has been very well solved, there are large individual differences in the classification accuracy of each BCI system (Ahn and Jun 2015).

Recently, studies focused on the physiological mechanism of MI-BCI, have become increasingly interesting. MI, which defines a mental rehearsal of movement without any actual motor output, results from interactions of many motor-related regions, such as the primary sensorimotor cortex (SM1), the supplementary motor area (SMA), and the basal ganglia (BG). As it has already been known, the loop including SMA, SM1 and BG forms the core part of MI (Jeannerod and Decety 1995; Decety 1996; Boecker et al. 1998; Munzert et al. 2009). Also, EEG and functional MRI (fMRI) studies have demonstrated the correlation between the BG–thalamus–cortex loop and MI-BCI performances (Birbaumer 2006). In general, the functional and structural interaction among the MI related circuit, including SM1, SMA, the thalamus and the BG (Pfurtscheller and Neuper 1997; Boecker et al. 2008; Kasess et al. 2008; Müller et al. 2013), is important for the achievement of MI-BCI.

Therefore, a possible assumption accounting for the individual differences in MI-BCI is that, rather than the MI ability, the difference in extraction of EEG features of above-mentioned regions may influence the classification of BCI to a large extent. For example, MI-related ERD feature and MI-BCI performance has close relationship. The clearer ERD, the higher MI-BCI accuracy could be achieved. However, not all subjects' EEG are good enough to extract a clear ERD when doing motor imagery. This assumption may explain why there is still a strong individual difference in BCI accuracy after a long-term MI training with real time feed-back of the Mu rhythm amplitude of each participant. According to the dipole-source model of EEG (Schimpf et al. 2002), the electrical field mapping on the scalp is not a simple overlay of all of the electrical fields from each neuron. The electrical fields derived from the gyrus activities are accumulated in the scalp and could be recorded easily by a scalp EEG. The counteractive nature of electrical fields of EEG recordings during activities in the sulci makes the activation in the sulci is difficult to be properly measured on the scalp, because of counteraction of potential in anisotropic electrical field.

In this study, we hypothesized that, the location (gyri or sulci) and the strength of MI-induced activation may affect the amplitude of ERD in the scalp EEG, thus interrupting the performances of MI-BCI, even if the MI was performed intently. As an essential substance of information interaction, white matter (WM) inter-connection within the loop associated with MI could provide an indirect approach to assess the cortical activity of MI. Based on our assumption, as the signals of electrodes C3 and C4 are most useful for MI-BCI, it is possible that the WM connections within this loop would mainly exist at the gyrus of the SM1 in subjects with a good MI-BCI performance. Also, the subject with higher MI-related WM connectivity in SM1 be found to have a better BCI performance. Thus, in this study, we examine our hypothesis by investigating that whether the WM connectivity features between the SM1 and the other regions in the MI loop would predict the MI-BCI performances. To achieve this, diffusion-weighted imaging (DWI) was used to reconstruct the white matter connection within the MI loop, including the SM1, SMA, three nuclei in the BG and the thalamus in a group of participants who were recruited to perform MI-BCI tests. Subsequently, the WM connectivity with the gyrus and the sulci of the SMA and the SM1 were evaluated, respectively. Finally, the connectivity features, such as the ratio of connection to the gyrus and the sulci, were as a result associated with MI-BCI performance.

Methods

Participants and Behavior Measure

Twenty-six volunteers (17 males and 9 females, mean age 22.96 ± standard deviation 1.97 years) participated in the

Table 1 Demographic information and motor imagery self-evaluating value of all participants

Variable	Mean	STD	Range
Age (years)	22.96	1.97	19–26
Gender	Female = 9		
Handedness	Right-handed		
MIQ-RS_V	4.56	0.43	3.7–5
MIQ-RS_K	4.46	0.46	3.4–5
KVIQ_V	6.44	0.61	5–7
KVIQ_K	6.03	0.70	4.57–7

STD standard deviation, *MIQ-RS_V* and *MIQ-RS_K* visual and kinesthetic imagery score of MIQ-RS questionnaire, respectively, *KVIQ_V* and *KVIQ_K* visual and kinesthetic imagery score of KVIQ questionnaire, respectively

study after signing informed consents. Subjects also underwent clinical psychiatric assessment and were confirmed to have no psychiatric or neurological disease history. Two left-handed subjects were eliminated after performing the Edinburgh Handedness Inventory. Each participant finished two simple questionnaires (MIQ-RS and KVIQ-20) (Malouin et al. 2007; Gregg et al. 2010) to make sure that each one of them have the ability to do motor imagery (Table 1). These questionnaires, interned reflect self-identified motor imagery ability, constituting self-rating of visual and kinesthetic motor imagery. The study was approved by the ethics committee of the University of Electronic Science and Technology of China.

EEG Data Acquisition and Processing

EEG data were recorded with 15 Ag/AgCl electrodes from an extended 10–20 system by using a Symtop amplifier (Symtop Instrument, Beijing, China); for more details, refer to our previous study (Zhang et al. 2015). Subjects performed left/right hand MI according to the instructions on the computer screen. Trials begun with a 4 s rest period, a cue then appeared on the left or right side of the screen for 1 s to instruct the subject to perform MI with the left or right hand. After the bar turned green, the subjects performed the requested motor imagery for 5 s. The motor imagery dataset included four runs, the first two runs of which as the training set and the last two runs as the test set, for each subject, with 50 trials per run.

A standard pipeline was used to analyze the EEG data of the BCI experiments. The 15 electrodes were selected from extended 10–20 system, which covered the whole brain (Fig. S1). In brief, the MI-BCI performance, which was characterized by the MI-BCI recognition rate, of each subject was obtained from their motor imagery dataset. Furthermore, common spatial patterns were used to extract the motor imagery-related EEG features, and linear discriminant analysis was used to classify the left/right hand motor imagery conditions based on the extracted features (Zhang et al. 2015). SMR, which reflects motor imagery-related changes in EEG activity, was used to divide different types of imagined movements. For calculating motor imagery-related ERD, the 2 s EEG segment before the cue was considered as the baseline period, as event-related changes in ongoing EEG require time to recover, and the 5 s EEG segment during motor imagery was considered as a task period. According to previous MI-BCI literatures (Blankertz et al. 2010), the MI-related ERD occurs mainly at channel C3 and C4, thus in this study, Laplacian-filtered C3 and C4 channels were selected for calculating the ERD [Laplacian-filtered C3 signal is calculated from C3-1/4(FC3 + C5 + CP3 + Cz), and Laplacian-filtered C4 signal is calculated from C4-1/4(FC4 + C6 + CP4 + Cz)], and an 8–30 Hz (consisting of an 8–30 Hz motor imagery related-MU rhythm and a 16–26 Hz BETA rhythm) power for the baseline and task periods, were first obtained by the fast Fourier transform method. The ERD of one trial was calculated according to the method described in (Jeannerod and Decety 1995). Finally, the ERD was averaged across the trials. Moreover, it must be mentioned that, the lower the ERD value is, the higher the activation of the corresponding region (Table 2).

MRI Data Acquisition

All MRI data were obtained using a GE 3 T scanner (GE Discovery 750) with a standard 8-channel head coil (GE Medical Systems, Milwaukee, WI) in the MRI research center of UESTC. The subjects lay supine on the scanner bed, and visual stimuli were back-projected onto a screen through a mirror built into the head coil. For each subject, diffusion-weighted images were acquired using a single-shot, spin-echo, echo-planar sequence (TR = 8500 ms; TE = 70 ms; voxel size = 2 × 2 × 2 mm^3; FOV = 256 × 256 mm; 76 axial slices; scan time = 10 min; diffusion direction = 64; b factor = 1000 s/mm^2). In addition, before the acquisition of DWIs, we acquired 3

Table 2 BCI performances

Variable	Mean	STD	Range
BCI accuracy ratio	0.764	0.136	0.52–0.99
ERD in C4 of β (left MI)	−0.035	0.121	−0.355–0.318
ERD in C4 of μ (left MI)	−0.076	0.162	−0.427–0.361
ERD in C3 of β (right MI)	−0.046	0.106	−0.282–0.228
ERD in C3 of μ (right MI)	−0.089	0.121	−0.285–0.227

Left MI means ERD value when doing left-hand motor imagery and right MI means ERD value when doing right-hand motor imagery

STD standard deviation

non-diffusion-weighted data sets as a reference. High resolution 3D FSPGR T1 images were acquired for each subject with a matrix = 256 × 256 × 152 and a voxel size = 1 × 1 × 1 mm^3.

Preprocessing of Diffusion MRI Data

First, motion and eddy current corrections were performed for each subject's diffusion MRI (dMRI) data by linear registering of all DWIs to the averaged image of 3 non-diffusion-weighted images (Fig. 1, step 1). After this, global registration was carried out for the dMRI data to the T1 anatomy by using rigid-body transformation (FLIRT tool in FSL 5.0.6, http://www.fmrib.ox.ac.uk/fsl; FMRIB Software Library, University of Oxford) (Jenkinson et al. 2012), followed by gradient direction transformation using the rotation parameters. This process also interpolated all DWIs to the individual anatomy space by tri-linear interpolation.

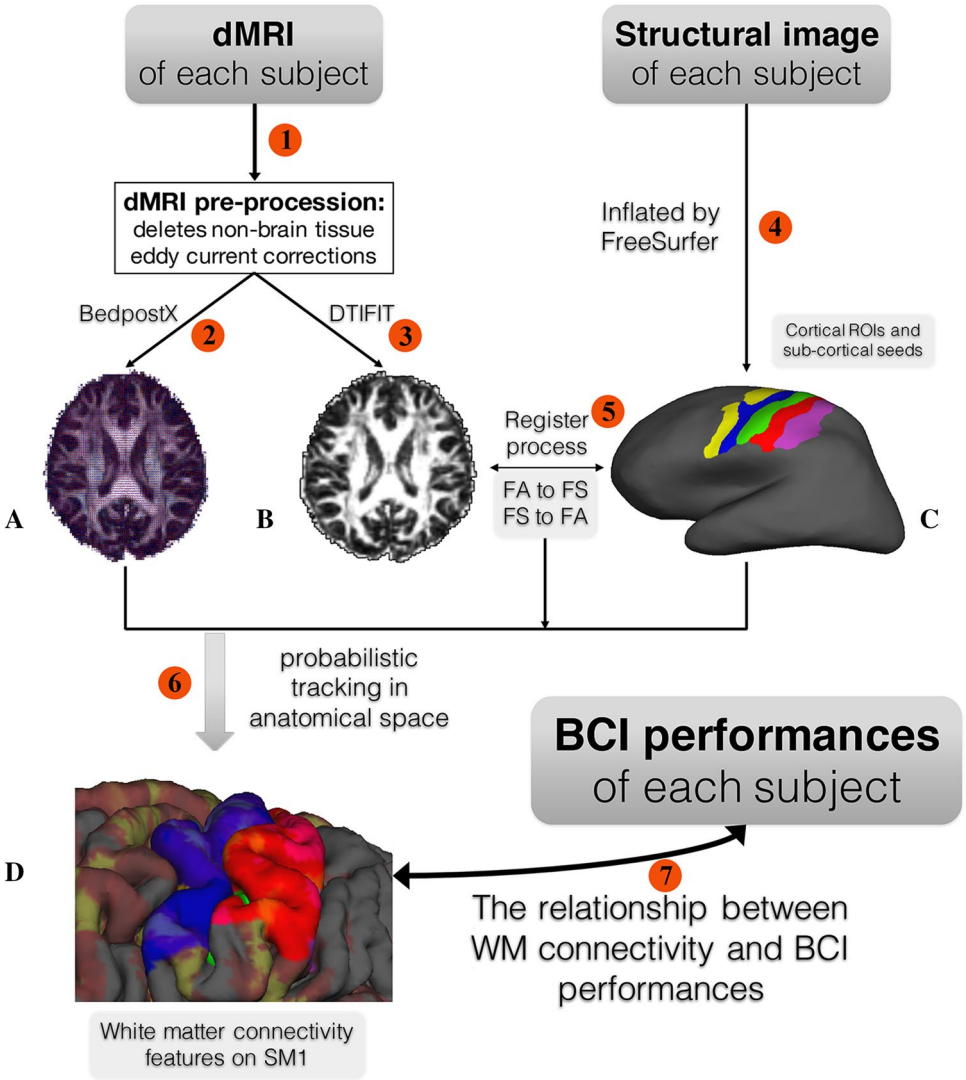

Fig. 1 Flow chart. *Step 1* dMRI of every subject were preprocessed. The preprocessing included deleting non-brain tissues and eddy current corrections; *Step 2* a diffusion tensor mode was applied to reconstruct FA map (*a*, by DTIFIT tool); *Step 3* a Markov Chain Monte Carlo sampling was used to build up distributions on the diffusion parameters at each voxel (*b*, by BedpostX tool); *Step 4* structural image of each subject was inflated by FreeSurfer. And a neuroanatomical label was assigned automatically to each location on a cortical surface model based on probabilistic information estimated from a manually labeled training set. ROIs, such as gyri and sulci of SM1, were extracted from Destrieux Atlas (*c*, sulci of precentral was shown in *yellow*, gyrus of precentral in *blue*, central sulcus in *green*, gyrus of postcentral in *red* and sulcus of postcentral in *violet*). *Step 5* Transformation matrixes, which was between FreeSurfer space and FA map, was acquired. *Step 6* Tractograms were acquired in anatomical space by probabilisitic tracking which using BG, SMA, CI and CC as seeds. White matter connectivity features, including connectivity strength and connectivity GSR, on SM1 was acquired (*d*, overlaid the tractogram of BG, which was shown in *yellow–red*, on pial surface.). *Step 7* The relationship between WM connectivity features and BCI performances was investigated. (Color figure online)

There are two inherent advantages of transforming the diffusion images and the corresponding gradient directions to the anatomical space, even though this process increases the calculation complexity. Registration to the anatomical space made it possible to acquire tractograms, which were reconstructed by using the refined segmentation of the individual anatomical image as seed. Smoothing was introduced to the images caused by the interpolation step of the rigid transformation. Therefore, this would reduce a potential directional bias, which might be caused by the interpolation for the different dMRIs in the motion correction procedure. This procedure was tested and verified by work from Professor Anwander and his colleagues (Ruschel et al. 2013). Most importantly, as Smith has mentioned, there is no significant interpolation blurring introduced into the images by performing the procedure described above (Smith et al. 2006).

After registration, a diffusion tensor mode was applied to reconstruct diffusion parameter maps, such as fractional anisotropy (FA) or mean diffusivity (MD). Subsequently, a Markov Chain Monte Carlo sampling was used to build up distributions of the diffusion parameters at each voxel, in which we hypothesized that there were no more than 2 families of fibers (Behrens et al. 2007) (Fig. 1, step 2, 3).

Definition of the Region of Interest

Twenty-two regions of interest (ROIs) associated with motor imagery were identified according to the meta-analysis by Hétu et al. (2013), including 12 SM1 regions (the bilateral gyrus of the precentral region, the gyrus of the postcentral region, the sulcus of the central region, the superior and inferior sulcus of the precentral region, and the sulcus of the postcentral region), two SMA regions (bilateral SMA), six BG regions (bilateral caudate nucleus, putamen, and pallidum) and two thalamic regions (bilateral thalamus) (Fig. 1, step 4). These ROIs, except for SMA, were acquired by segmented native anatomic images using FreeSurfer (http://surfer.nmr.mgh.harvard.edu; Martinos Center for Biomedical Imaging, Boston, USA) according to the Destrieux cortical atlas. To acquire tractograms more reliably and to avoid a partial volume effect, we constrained the cortex ROI masks using individual FA between 0.15 and 0.25, which was considered as the gray–white matter interface (Ruschel et al. 2013). Similarly, to exclude the external capsula and internal capsula from the basal ganglia and thalamic ROIs, we excluded voxels of which FA value higher than 0.6 from these ROIs. We manually defined the SMA ROIs as follows because there is no firsthand SMA mask in the Destrieux Atlas. First, BA 6 was identified for each subject. We then extruded the SMA ROI by excluding the primary and pre-motor areas from BA 6, as BA 6 is composed of a pre-motor area, SMA and a primary motor area. Finally, we checked the SMA ROI of each subject by eye.

Moreover, considering that there might be a relationship between the ERDs and the WM connectivity between the bilateral hemispheres, the WM connectivity on the corpus callosum (CC) tract was considered. We only focused on the one part of the CC that connected the bilateral SM1. To map this part, we drew the entire CC mask manually for each participant and constrained it using FA >0.3. These masks were used as seeds to reconstruct probabilistic tractography, and bilateral SM1 masks (including the bilateral precentral and postcentral regions) were used as classification targets. After the probabilistic tractography, we obtained the output classification images. The value of each voxel in the classification images was the number of samples, which started from the voxel and reached the SM1 mask. Subsequently, we binarized these classification images by the stronger 50% non-zero voxels to acquire the SM1 part of CC.

Most importantly, these ROIs were used as seeds for probabilistic fiber tracking in the following analysis.

Tractography and Connectivity Analysis

Probabilistic tractography method (probtrackx script in FSL) (Behrens et al. 2007) was used to reconstruct whole brain WM connectivity maps using each sub-cortical area, the SMA area and the SM1 part of the CC as seeds (Fig. 1, step 6). Due to the fact that the connectivity distribution dropped with distance from the seed mask, distance correction was used in the tractography reconstruction procedure. Furthermore, 10,000 iterations of tracking were performed for each voxel in each seed to get tractograms more reliably. Specifically, as the thalamus is an important relay for sensory motor information, we reconstructed the BG-cortical WM connections in which the bilateral thalamus served as the waypoint ROIs (Figs. 2, S2, S3).

The WM pathway contained in the corticospinal tracts (CST) is observed to be related to motor execution instead of MI. Therefore, similarly, the anterior and posterior arms of the internal capsule were defined as seed. Subsequently, the bilateral CST were acquired by probabilistic tracking between the internal capsule and the SM1.

After probabilistic tracking, connectivity distribution maps were binarized by the stronger 30% non-zero voxels to acquire mean FA and MD values of each participant on all tracts. Then, the connectivity strength and connectivity pattern between the ROIs were calculated. Connectivity strength S (A, B) was defined by the formula

$$S(A,B) = \frac{\sum P_A(R_B) + \sum P_B(R_A)}{V_A + V_B}$$

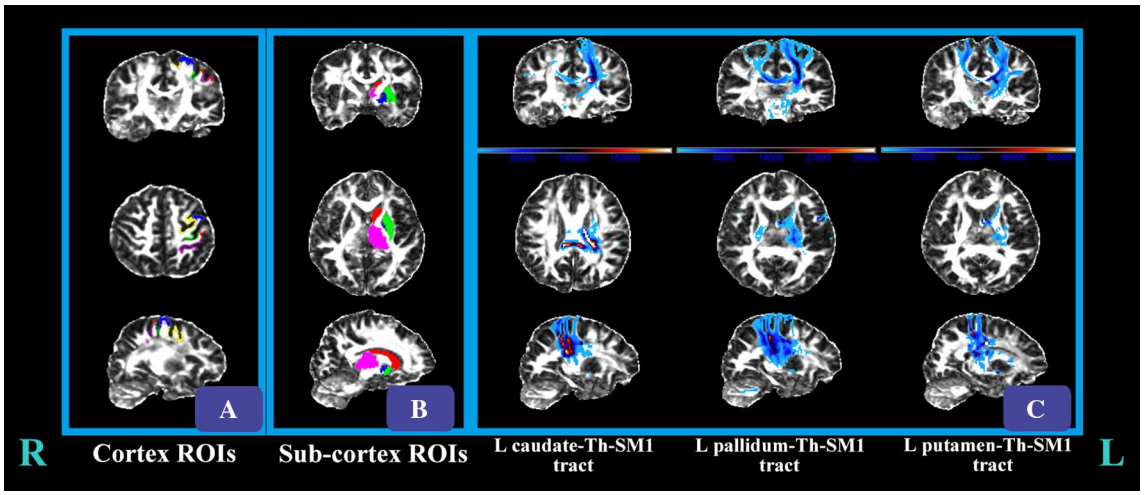

Fig. 2 ROIs and tractograms of BG and SM1 (only showed *left* hemisphere). *a* Overlaid SM1 ROIs on FA map (sulci of precentral was shown in *yellow*, gyrus of precentral in *blue*, central sulcus in *green*, gyrus of postcentral in *red* and sulcus of postcentral in *violet*). *b* Overlaid sub-cortical seeds on FA map (thalamus was shown in *pink*, caudate shown in *red*, putamen was shown in *green* and pallidum was shown in *blue*). *c* Tractograms which were acquired by using BG as seeds and ipsilateral thalamus as waypoint. (Color figure online)

where the $\sum P_A(R_B)$ represents the total streamlines from seed region A that reached target region B after 10,000 random walks and V_A represents the number of voxels in region A.

Meanwhile, the connectivity pattern "Gyrus-Sulcus Ratio (GSR)" was defined on the ratio of S (Gyrus, A) and S (Sulcus, A), where Gyrus denotes gyrus ROIs in SM1, Sulcus denotes sulcus ROIs in SM1, and A implies the seed ROIs. This indicator can reflect the projection pattern of the MI-related fiber bundle at SM1.

In this study, we obtained the connectivity strength and the GSR on SM1 of WM pathways including BG-thalamic-SM1 and SMA-SM1 loops. Subsequently, correlations were calculated between the BCI performances and the WM characteristics, including FA/MD on tract and connectivity strengths, as well as connectivity patterns (GSR) across all 24 subjects (Fig. 1, step 7). Subsequently, the difference in WM characteristics mentioned above between the higher and the lower BCI performance groups were compared using a Mann–Whitney U test.

Support Vector Regression (SVR) Analysis

After obtaining the single influence of these WM characteristics on the MI-BCI, the coupling effect of a given WM tract characteristics on the on-line BCI accuracy, were also analyzed. A supervised learning technique deriving from the support vector machines (SVM) to predict continuous variables, as a usual SVR (ε-SVR) algorithm (Smola and Schölkopf 2004), was used to predict the individual BCI accuracy by WM mixed features. Features were selected based on the abovementioned correlation results. We normalized the WM characteristics, which were found to be correlated with BCI performances, to the [0 1] range divided by the maximum. The SVR training were conducted using the LIBSVM (Library for Support Vector Machines) toolbox (Chang and Lin 2011) implemented in MATLAB (R2013b; The MathWorks, Natick, MA). Then the regression model was evaluated using a leave-one-out cross-validation procedure, and used for prediction of the on-line BCI accuracy. After the predicting of BCI accuracy, the correlation coefficient between predicted BCI accuracy and the actual one for all participants was calculated. Subsequently, permutation based nonparametric statistic method was used to disprove the null hypothesis that, there is no correlation between actual and predicted BCI accuracy by the randomly disrupted order of actual BCI accuracy of all participants in each iteration. The significant level was defined by the proportion of permutations that the original correlation coefficient was smaller than the 5000 iterated ones. Finally, we used the mean absolute error (MAE) (Franke et al. 2010) to measure the correctness of the BCI accuracy estimations.

Results

BCI Performances

Because MI ability might be affected by handedness, we excluded two left-handed participants from further analysis.

According to the calculation of the EEG data, we obtained five types of BCI performances for each subject, which included BCI online accuracy, ERD on the C3

electrode in Mu rhythm and in Beta rhythm when doing right hand MI, as well as ERD on the C4 electrode in Mu rhythm and in Beta rhythm when doing left hand MI.

Based on the BCI accuracy, the 24 subjects were equally divided in to 3 groups, where the higher threshold was 0.8 and the lower was 0.75. This grouping was aimed to highlight the intergroup difference of the WM features. After eight higher-performance subjects and eight lower-performance subjects were assigned to their own groups, respectively, the remainders were assigned to the middle group, which were excluded from the comparison process between the other two groups, as the middle-performance group had some ambiguous factors.

The Fiber Tracking of MI-Related Pathways

We checked the tractography results of BG (Fig. 2), the SM1 part of CC (Fig. S2) and CI (Fig. S3) for each subject to ensure the reliability of further analysis. After this, we obtained the WM connectivity characteristics, as well as the microstructure characteristics of each tract. Then, we discovered that, some white matter connectivity characteristics were associated with BCI performances.

Association of BCI Performances with WM Between the BG and Cortical Regions Where the Thalamus was the Waypoint

In the condition where the thalamus was used as the waypoint, five significant associations were found between BCI performances and white matter characteristics, which were between the BG and the cortical regions ($P < 0.01$, uncorrected). Three of them were negative correlations between the ERDs and the three GSRs (between the right caudate and the precentral region, between the left pallidum and the SM1, and between the left pallidum and the precentral region). The remaining two were positive correlations, which were between the BCI accuracy and the two GSRs (between the right caudate and the precentral region and between the right putamen and the precentral region). Unfortunately, no WM connectivity strengths were found to be significantly correlated with BCI performances (Fig. 3; Table 3). In addition, the MD on tract between the right pallidum and the postcentral region, with the thalamus as the waypoint, was found to positively correlate with the ERD value on the C4 electrode in the Mu band when doing left MI (Fig. S4; Table S1).

Association of BCI Performances with WM Characteristics on the SM1 Part of the CC Tract

We discovered that, the connectivity strength on the SM1 part of the CC tract significantly and negatively correlated with the ERD values on the C3 electrode when doing right MI and on the C4 electrode when doing left MI. These results were also consistent with our hypothesis (Fig. 4; Table 4).

Association of BCI Performances with WM Mixed Features in the MI Loop

When the four GSRs of the BG-Th-SM1 WM connectivity, which showed significant correlation with ERDs and with BCI accuracy, were used in combination as input samples, an estimation accuracy was obtained. The correlation between the estimated and the actual BCI accuracy of subjects was $r = 0.56$ (Fig. 5), with the significant level $P < 0.05$ (nonparametric test). The MAE between the estimated and true accuracy was 0.1.

In a word, the WM connectivity characteristics, including connectivity strength, connectivity patterns and WM microstructure measurements between the BG and the SM1, were found to correlate with BCI performances. In addition, using a combination of specific white matter characteristics as a mixed feature, we can predict the MI-BCI accuracy of the subjects. However, the WM characteristics, which was reconstructed from the thalamus (as seed) and the SMA to the SM1, did not show a significant correlation with BCI performances.

Discussion

The potential structural and functional coupling may play a role in information processing in the human brain (Blankertz et al. 2010; Halder et al. 2013). In this study, we provided the further evidence to support that, the white matter pathway characteristics including the connectivity strength and the connectivity patterns (GSR) have a significant impact on EEG signals during MI. In addition, consistent with our hypothesis, this study illustrated that subjects who have distinct WM connections between the gyri of SM1 and BG (high GSR) linked to higher MI-BCI performances than those who have more WM connections between the sulci of SM1 and BG. To the best of our knowledge, this is the first study to suggest that WM connectivity pattern between the cortical (SM1) and subcortical (BG) regions plays a role in the evaluation of BCI performances. Moreover, this study may afford indirect non-invasive evidence to support that, the activation at the sulci causes poor detection of EEG features related to MI tasks.

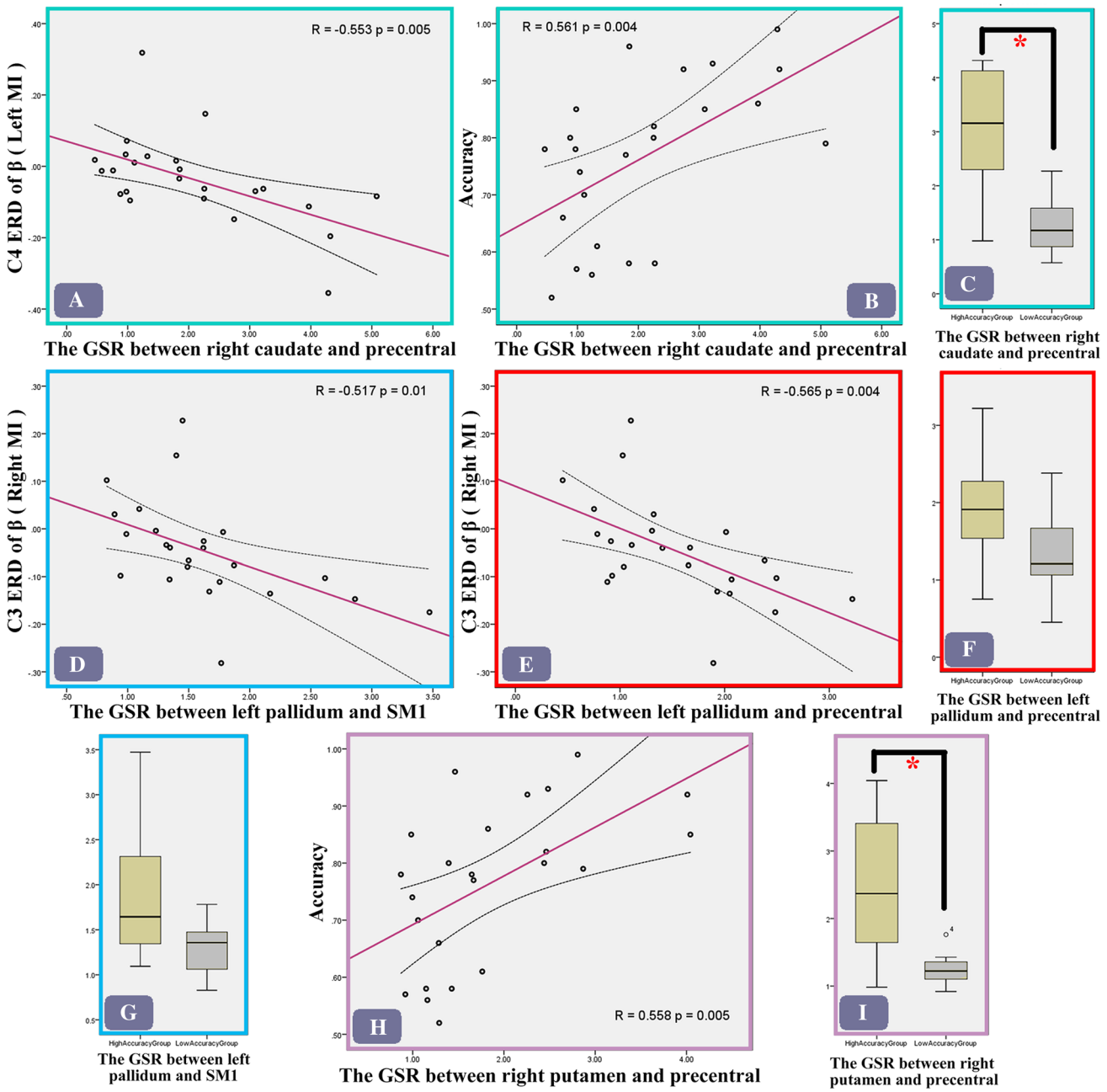

Fig. 3 Significant associations between BCI performances and white matter characteristics, which were between the BG and the cortical regions, acquired in the condition where the thalamus was used as the waypoint. *Boxplots* reflected distributions on WM characteristics of same-colored scatterplot of high accuracy group (in *yellow*) and low accuracy group (in *grey*). *Asterisk* in *boxplots* means that WM characteristics of two groups showed significant differences. (Color figure online)

The Pattern (GSR) of the WM Connection of the SM1 with the BG Plays a Critical Role in the Detection of ERDs

The successful identification of EEG signal features related to MI is crucial in MI-BCI. Neuronal activation at the cortex, especially at the gyri rather than the sulci, mainly contributes to the signal recorded in the scalp EEG. Thus, the activation ratio of the gyri and the sulci (GSR) during MI could predict the efficiency of detecting the EEG signal of MI. The WM connection between the regions in the MI loop plays a role in information integration. In a previous study, this loop, including the SM1, the SMA, the BG and the thalamus, has been observed to be part of the activation induced by the MI task. In this study, we found that, rather than WM connectivity strength itself, the GSR of the

Table 3 White matter connectivity characters between BG and SM1 when thalamus was used as waypoint

Seeds	Targets	Connectivity strength			GSR		
		Mean	STD	Correlation	Mean	STD	Correlation
Caudate	L_Pre	16941.59	10051.43		1.34	0.89	
	R_Pre	10202.54	12032.11		2.05	1.33	C4 ERD↓ Accuracy↑
	L_Post	27988.69	24465.33		2.09	1.53	
	R_Post	11347.06	12719.80		1.07	0.71	
	L_SM1	20253.30	11003.88		1.45	0.72	
	R_SM1	10520.79	10330.05		1.56	0.92	
Pallidum	L_Pre	4891.85	2716.79		1.54	0.69	C3 ERD↓
	R_Pre	2901.53	2563.41		1.67	0.74	
	L_Post	5390.90	4124.96		2.18	1.62	
	R_Post	2972.47	2954.63		1.48	1.25	
	L_SM1	5013.23	2812.36		1.63	0.63	C3 ERD↓
	R_SM1	2921.75	2470.08		1.50	0.65	
Putamen	L_Pre	6936.30	10485.58		1.46	0.74	
	R_Pre	9477.30	8592.40		1.84	0.91	Accuracy↑
	L_Post	10104.23	12740.52		1.92	1.18	
	R_Post	9090.10	7882.35		1.27	0.90	
	L_SM1	11166.61	7576.84		1.55	0.65	
	R_SM1	8398.45	8871.74		1.56	0.67	

STD standard deviation, *L_Pre* left precentral, *R_Pre* right precentral, *L_Post* left postcentral, *R_Post* right postcentral, *L_SM1* left primary sensorimotor areas, *R_SM1* right primary sensorimotor areas

"↑" means significant positive correlation; "↓" means significant negative correlation

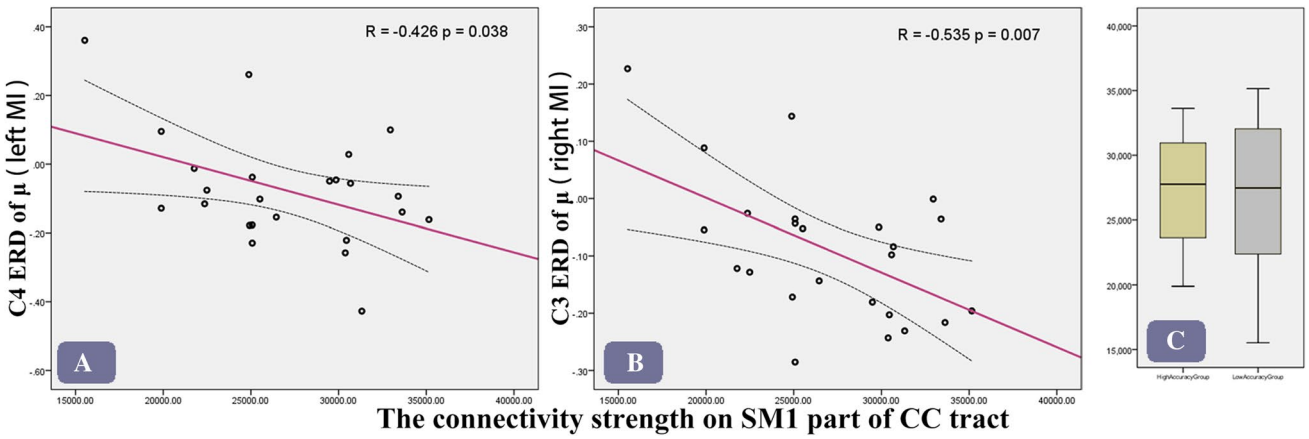

Fig. 4 Connectivity strength on the SM1 part of the CC tract significantly correlated with BCI performances

Table 4 White matter connectivity characters on corpus callosum tract between bilateral SM1

Variable	Target	Seed	Mean	STD	Correlation
Connectivity	SM1	SM1 part of corpus callosum	26949.64	5081.65	C3 ERD↓, C4 ERD↓

STD standard deviation

"↑" means significant positive correlation; "↓" means significant negative correlation

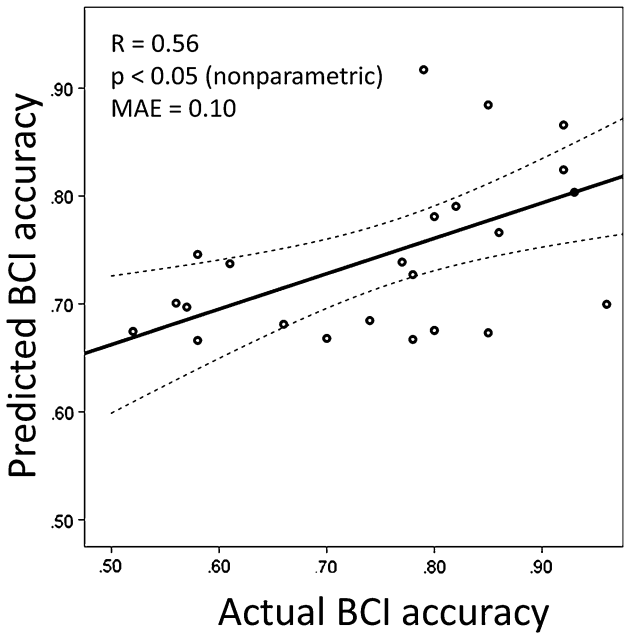

Fig. 5 Four WM connectivity characteristics, including the GSR between right caudate and precentral, the GSR between left pallidum and precentral, the GSR between left pallidum and SM1 and the GSR between right putamen and precentral, which were found correlated with BCI performances, were introduced to SVR process to predict BCI accuracy. The scatter plot showed the correlation (estimation accuracy $r = 0.56$, $P < 0.05$ by permutation based nonparametric test, and the MAE = 0.10.) between the SVR estimated and the actual BCI accuracy of subjects

tract linked to the BG on SM1was associated with the MI-BCI performances. According to the white matter anatomy of the human brain, some efferent connections of BG connects to SM1 through the thalamus. Consisted with our hypothesis, when the thalamus was included as a relay in the WM fiber tracking, a better ERD detection and a higher BCI accuracy was found correlated with a higher GSR of the BG-SM1 tracts on the SM1. Therefore, these findings suggested that the GSR of the WM connection between the SM1 and the BG plays an imperative role than the WM connection between the whole SM1 and the BG.

In our findings, the caudate nucleus was a main component in the WM connection between the BG and the SM1 that contributed to the prediction of MI-BCI performance. In general, the caudate nuclei are involved in the encoding process of motion response and spatial working memory (Postle and D'Esposito 1999) and play an important role in motor functions such as adjusting the posture of the limbs and modulating speed and accuracy in motor functions (Villablanca 2010). All the participants were asked to imagine their hands waving like slapping a ball with a 1 Hz frequency when they interacted with the MI-BCI system online. In this process, the caudate nuclei would play a modulation role in the interaction between the sensory and the motion information. Combining our findings related to the caudate nuclei, these goes to suggest that the caudate takes part in the MI as a major component in the BG. A further analysis of the SM1 through its division into pre- and postcentral regions revealed that the precentral region, which responds to the motor function, was a major contributor in our results. It is hence likely that the MI is related to the WM connection between the primary motor cortex (precentral region of SM1) and the caudate nuclei. In addition, we observed that the right connection between the caudate and the SM1 was a better predictor than the left. Similarly, the ERD of the rhythm at C4 (right hemisphere) was also related to the right WM connection. This seems to suggest a lateralization in the effect of the WM connection on MI performance in our study. In other words, detecting the imagery of the left limb movement (activation at the left SM1) might be easier than the imagination of the right. We presumed therefore that, the right handedness of subjects might associate with the potential lateralization observed here, as a more significant ERD feature was observed in the left limb MI than in the right limb MI in a previous EEG study (Stinear et al. 2006; Nam et al. 2011).

Depending on previous studies, putamen and primary motor cortex takes part in motor planning and preparation (Deiber et al. 1996; Taniwaki et al. 2003; Gerardin et al. 2004). In detail, in motor preparation process, sensorimotor cortex activated first, and then output information to putamen. After received information from SM1, these information has been processed in putamen, and have been sent back to SM1 through the thalamus (Petrides et al. 1989; Alexander and Crutcher 1990). These information interactions were supported by the WM pathways between the above-mentioned regions. In the present, it has been found that the GSR of the left putamen-cortex pathway on precentral was positively correlated with BCI accuracy. This result may reveal the process, that precentral motor cortex activated and transmitted motor preparation information to putamen in motor imagery process, and this activation has been recorded by EEG to achieve BCI, was effected by the WM connectivity between these regions.

Pallidum is part of the extrapyramidal motor system. In primates, it is divided into two parts: internal globus pallidus (GPi) and the external globus pallidus (GPe). As a part of BG, GPe receives information from striatum and then project to GPi through subthalamic nucleus. After that information was relayed by thalamus and output to cortex. In addition, GPi involves in direct pathway, receive information from striatum and output to thalamus. In this study, the significant correlations were found between ERDs and the GSR of the pallidum-seeded pathways on cortex. These results demonstrated that the pallidum-cortical WM

connection was involved in the process of motor imagery, and their WM characteristics play a significant role in the generation of the MI-induced ERDs.

In addition, SVR results demonstrated that the WM mixed features of BG–thalamus–SM1 loop could predict the BCI accuracy. This indicated that the information interaction in BG–thalamus–SM1 loop was important in MI progress, and gave more evidence that EEG signal is affected by the WM connectivity characteristic of human brain. Based on the results of the SVR, we have raised the possibility that all parts of the BG in a collaborative way to participate in the process of motor imagery, and their WM connections to cortex could affect the accuracy of BCI. However, the role of each part of BG for MI was unclear, and need further studies.

The Participation of the SMA in MI-BCI

The signal at the C3 and C4 electrodes, which are close to the SM1 and the SMA, is commonly used for analysis in MI-BCI. Therefore, in our assumption, the GSR connection of WM in the SM1 and the SMA might influence the detection of ERDs related to MI. The SMA contributes to the control of movement, inhibition of movement, and the initiation of internally generated movement (Nachev et al. 2008). The neuronal assemblies in the SMA and the SM1 are related to complex cognitive processes, especially the motor-related information process (Georgopoulos et al. 1993). However, we didn't find any significant correlation between BCI performances and WM characteristics existing between SMA and SM1. We speculate that was because, the SMA and SM1 are all cortical regions, and the dMRI was not sensitive enough to reconstruct small nerve fibers between cortices.

The Relationship Between ERD and Interhemispheric Coupling

The corpus callosum, which connects the bilateral cerebral hemispheres and facilitates interhemispheric communication, was thought to serve both an inhibitory and excitatory influence on the contralateral hemisphere (Meyer et al. 1998; Bloom and Hynd 2005). Thus, the structural connectivity of the corpus callosum may affect the discrimination in ERD amplitude during motor imagery of different hands, which in turn affects the accuracy of BCI. In this study, it's found that the connectivity strength on the SM1 part of the CC tract significantly and negatively correlated with the ERD values. This result reflects the stronger the structural connection between hemispheres, the higher the EEG activation of MI. One possible explanation of this finding is that the structural connectivity between the hemispheres may affect the inhibition of irrelevant side SM1 at the MI task, then impact on the ERD. However, this speculation requires further study to verify.

The Role of CST in MI-BCI Performance

CST mainly arise from the primary motor cortex, supplementary motor area, premotor cortex, and somatosensory cortex, and control the movement of muscles of the body (Hall 2015). CST carries motor information from the primary motor cortex to the motor neurons in the spinal cord. We did not find any significant correlation between BCI performance and white matter characteristics of the CST pathway. The MI-related information is only a small part of these, and hence, it is comprehensible that there was no significant correlation between them.

Limitations and Prospects

EEG has high temporal resolution and is sensitive to a change in cortical potential so that it can recognize whether the cortex is activated or not. The activation signal was recorded in the C3 and C4 electrodes when motor imagery was used to operate BCI system. In order to stabilize the data quality, we did our best to maintain the consistency for each participant of a variety of features, including but not limited to the experimental environment, equipment, instruction, training duration, smearing of electrode jelly, and wearing of the electrode cap. Thus, it can be considered that the individual differences in BCI performance correlated with only the participants themselves.

DMRI measures the dephasing of the spins of protons in the presence of a spatially-varying magnetic field. This measurement, which was used to estimate fiber orientation density function, only reflects the amount of hindrance when water molecules are moving with a component of displacement along the direction of the applied gradient, which is then averaged over the voxel. Therefore, the derived tractogram did not acquire the actual anatomical connectivity. This leads to false-positive and false-negative connections in the tractograms. Besides, the issue of crossing fiber would still be a major problem disturbing findings of dMRI. This problem has not been well resolved under the existing technical framework. To ensure data quality, we examined the original dMRI image for each subject, corrected the effects of distortion caused by eddy current and susceptibility by using the EDDY toolkit of FSL, checked the registration results and used more iterations in the tracking stage. Therefore, despite these limitations, the accuracy of the estimation of the long-range connectivity is enough to be considered as an indicator of anatomical connectivity.

In addition, a study of Tal and colleagues demonstrated that fractional anisotropy of particular white matter tracts

are associated with auditory-motor synchronization skills (Blecher et al. 2016). Although there's no significantly correlation between MI-related WM connectivity strength in SM1 with BCI performance and with EEG feature found in the present, we speculated that WM connectivity may also have an impact on the ability of motor imagery. The negative result of this study may be due to the fact that we only focus on the WM connectivity on SM1, rather than the entire MI-related tracts. We will investigate this issue in the future.

Conclusion

To the best of our knowledge, the present study demonstrates the potential relationship between the WM pathway of the human brain and EEG signals in MI performances for the first time. The pattern of WM connectivity of the BG-SM1 has a great influence on both EEG signal and the classification accuracy in MI-BCI. These results indicated that the BG-SM1 WM connection participates in the MI process and that the connectivity characteristics of these connections have an impact on the generation of the MI-related EEG signal. In summary, we provided the coupling mechanism between structural and dynamic physiology features of human brain, which would associate with the underlying reason for MI individual differences. This study also provides some supporting material for the researches of the origin of EEG.

Acknowledgements This study was funded by grants from the National Nature Science Foundation of China (81330032), the PCSIRT Project (IRT0910), and Special-Funded Program on National Key Scientific Instruments and Equipment Development of China (2013YQ49085908).

Compliance with Ethical Standards

Disclosures None of the authors has any conflict of interest to disclose. We confirm that we have read the Journal's position on issues involved in ethical publication and affirm that this report is consistent with those guidelines.

References

Ahn M, Jun SC (2015) Performance variation in motor imagery brain–computer interface: a brief review. J Neurosci Methods 243:103–110. doi:10.1016/j.jneumeth.2015.01.033

Alexander GE, Crutcher MD (1990) Preparation for movement: neural representations of intended direction in three motor areas of the monkey. J Neurophysiol 64(1):133–150

Behrens TEJ, Berg HJ, Jbabdi S et al (2007) Probabilistic diffusion tractography with multiple fibre orientations: what can we gain? NeuroImage 34:144–155. doi:10.1016/j.neuroimage.2006.09.018

Birbaumer N (2006) Breaking the silence: brain? Computer interfaces (BCI) for communication and motor control. Psychophysiology 43:517–532. doi:10.1111/j.1469-8986.2006.00456.x

Blankertz B, Sannelli C, Halder S et al (2010) Neurophysiological predictor of SMR-based BCI performance. NeuroImage 51:1303–1309. doi:10.1016/j.neuroimage.2010.03.022

Blecher T, Tal I, Ben-Shachar M (2016) White matter microstructural properties correlate with sensorimotor synchronization abilities. NeuroImage 138:1–12. doi:10.1016/j.neuroimage.2016.05.022

Bloom JS, Hynd GW (2005) The role of the corpus callosum in interhemispheric transfer of information: excitation or inhibition? Neuropsychol Rev 15:59–71. doi:10.1007/s11065-005-6252-y

Boecker H, Dagher A, Ceballos-Baumann AO et al (1998) Role of the human rostral supplementary motor area and the basal ganglia in motor sequence control: investigations with H2 15O PET. J Neurophysiol 79:1070–1080

Boecker H, Jankowski J, Ditter P, Scheef L (2008) A role of the basal ganglia and midbrain nuclei for initiation of motor sequences. NeuroImage 39:1356–1369. doi:10.1016/j.neuroimage.2007.09.069

Chang C-C, Lin C-J (2011) LIBSVM. ACM Trans Intell Syst Technol 2:1–27. doi:10.1145/1961189.1961199

Daly JJ, Wolpaw JR (2008) Brain–computer interfaces in neurological rehabilitation. Lancet Neurol 7:1032–1043

Decety J (1996) The neurophysiological basis of motor imagery. Behav Brain Res 77:45–52

Deiber MP, Ibañez V, Sadato N, Hallett M (1996) Cerebral structures participating in motor preparation in humans: a positron emission tomography study. J Neurophysiol 75:233–247

Franke K, Ziegler G, Klöppel S et al (2010) Estimating the age of healthy subjects from T1-weighted MRI scans using kernel methods: exploring the influence of various parameters. NeuroImage 50:883–892. doi:10.1016/j.neuroimage.2010.01.005

Galán F, Nuttin M, Lew E et al (2008) A brain-actuated wheelchair: asynchronous and non-invasive brain-computer interfaces for continuous control of robots. Clin Neurophysiol 119:2159–2169. doi:10.1016/j.clinph.2008.06.001

Georgopoulos AP, Taira M, Lukashin A (1993) Cognitive neurophysiology of the motor cortex. Science 260:47–52

Gerardin E, Pochon J-B, Poline J-B et al (2004) Distinct striatal regions support movement selection, preparation and execution. Neuroreport 15:2327–2331

Gregg M, Hall C, Butler A (2010) The MIQ-RS: a suitable option for examining movement imagery ability. Evid Based Complement Altern Med 7:249–257. doi:10.1093/ecam/nem170

Halder S, Varkuti B, Bogdan M et al (2013) Prediction of brain-computer interface aptitude from individual brain structure. Front Hum Neurosci 7:105. doi:10.3389/fnhum.2013.00105

Hall JE (2015) Guyton and Hall textbook of medical physiology. Elsevier Health Sciences, Philadelphia

Hétu S, Grégoire M, Saimpont A et al (2013) The neural network of motor imagery: an ALE meta-analysis. Neurosci Biobehav Rev 37:930–949. doi:10.1016/j.neubiorev.2013.03.017

Jeannerod M, Decety J (1995) Mental motor imagery: a window into the representational stages of action. Curr Opin Neurobiol 5:727–732

Jenkinson M, Beckmann CF, Behrens TEJ et al (2012) FSL. NeuroImage 62:782–790. doi:10.1016/j.neuroimage.2011.09.015

Kasess CH, Windischberger C, Cunnington R et al (2008) The suppressive influence of SMA on M1 in motor imagery revealed by fMRI and dynamic causal modeling. NeuroImage 40:828–837. doi:10.1016/j.neuroimage.2007.11.040

Kubler A, Nijboer F, Mellinger J et al (2005) Patients with ALS can use sensorimotor rhythms to operate a brain-computer interface. Neurology 64:1775–1777. doi:10.1212/01.WNL.0000158616.43002.6D

Malouin F, Richards CL, Jackson PL et al (2007) The kinesthetic and visual imagery questionnaire (KVIQ) for assessing motor imagery in persons with physical disabilities: a reliability and construct validity study. J Neurol Phys Ther 31:20–29. doi:10.1097/01.NPT.0000260567.24122.64

Meyer BU, Röricht S, Woiciechowsky C (1998) Topography of fibers in the human corpus callosum mediating interhemispheric inhibition between the motor cortices. Ann Neurol 43:360–369. doi:10.1002/ana.410430314

Müller K, Bacht K, Prochnow D et al (2013) Activation of thalamus in motor imagery results from gating by hypnosis. NeuroImage 66:361–367. doi:10.1016/j.neuroimage.2012.10.073

Müller-Putz GR, Daly I, Kaiser V (2014) Motor imagery-induced EEG patterns in individuals with spinal cord injury and their impact on brain–computer interface accuracy. J Neural Eng 11:035011. doi:10.1088/1741-2560/11/3/035011

Munzert J, Lorey B, Zentgraf K (2009) Cognitive motor processes: the role of motor imagery in the study of motor representations. Brain Res Rev 60:306–326. doi:10.1016/j.brainresrev.2008.12.024

Nachev P, Kennard C, Husain M (2008) Functional role of the supplementary and pre-supplementary motor areas. Nat Rev Neurosci 9:856–869. doi:10.1038/nrn2478

Nam CS, Jeon Y, Kim Y-J et al (2011) Movement imagery-related lateralization of event-related (de)synchronization (ERD/ERS): motor-imagery duration effects. Clin Neurophysiol 122:567–577. doi:10.1016/j.clinph.2010.08.002

Petrides M, Schwartz AB, Massey J (1989) Mental rotation of the neuronal populaton vector. Science 243:234–236

Pfurtscheller G, Neuper C (1997) Motor imagery activates primary sensorimotor area in humans. Neurosci Lett 239:65–68

Postle BR, D'Esposito M (1999) Dissociation of human caudate nucleus activity in spatial and nonspatial working memory: an event-related fMRI study. Brain Res Cogn Brain Res 8:107–115

Ramoser H, Muller-Gerking J, Pfurtscheller G (2000) Optimal spatial filtering of single trial EEG during imagined hand movement. IEEE Trans Rehabil Eng 8:441–446. doi:10.1109/86.895946

Ruschel M, Knosche TR, Friederici AD et al (2013) Connectivity architecture and subdivision of the human inferior parietal cortex revealed by diffusion MRI. Cereb Cortex. doi:10.1093/cercor/bht098

Schimpf PH, Ramon C, Haueisen J (2002) Dipole models for the EEG and MEG. IEEE Trans Biomed Eng 49:409–418. doi:10.1109/10.995679

Smith SM, Jenkinson M, Johansen-Berg H et al (2006) Tract-based spatial statistics: voxelwise analysis of multi-subject diffusion data. NeuroImage 31:1487–1505. doi:10.1016/j.neuroimage.2006.02.024

Smola AJ, Schölkopf B (2004) A tutorial on support vector regression. Stat Comput 14:199–222. doi:10.1023/B:STCO.0000035301.49549.88

Stinear CM, Fleming MK, Byblow WD (2006) Lateralization of unimanual and bimanual motor imagery. Brain Res 1095:139–147. doi:10.1016/j.brainres.2006.04.008

Taniwaki T, Okayama A, Yoshiura T et al (2003) Reappraisal of the motor role of basal ganglia: a functional magnetic resonance image study. J Nerosci 23:3432–3438

Valdés-Hernández PA, Ojeda-González A, Martínez-Montes E et al (2010) White matter architecture rather than cortical surface area correlates with the EEG alpha rhythm. NeuroImage 49:2328–2339. doi:10.1016/j.neuroimage.2009.10.030

Villablanca JR (2010) Why do we have a caudate nucleus. Acta Neurobiol Exp 70:95–105

Whitford TJ, Rennie CJ, Grieve SM et al (2006) Brain maturation in adolescence: concurrent changes in neuroanatomy and neurophysiology. Hum Brain Mapp 28:228–237. doi:10.1002/hbm.20273

Zhang R, Xu P, Chen R et al (2015) Predicting inter-session performance of SMR-Based brain–computer interface using the spectral entropy of resting-state EEG. Brain Topogr. doi:10.1007/s10548-015-0429-3